Porphyrinoids

Deutsche Ausgabe: DOI: 10.1002/ange.201603759
Internationale Ausgabe: DOI: 10.1002/anie.201603759

A Directly Fused Subporphyrin Dimer with a Wavelike Structure

Yasuhiro Okuda, Eiji Tsurumaki, Juwon Oh, Jooyoung Sung, Dongho Kim, and Atsuhiro Osuka**

Abstract: *[Ni(cod)$_2$]-mediated intramolecular reductive coupling of β–β′ linked meso,meso′-dibromosubporphyrin dimer gave the anti-isomer of meso–meso′, β–β′ doubly linked subporphyrin dimer as the first example of a fused subporphyrin dimer. The fused dimer* $\mathbf{3}_{anti}$ *displays an wavelike coplanar structure, a perturbed and red-shifted absorption spectrum, reversible redox behaviors with a decreased electrochemical HOMO–LUMO band gap, and a short* S_1*-state lifetime owing to the delocalized π-electronic network.*

Subporphyrinatoboron(III) complexes (hereinafter referred to as subporphyrins) are ring-contracted porphyrins housing a central boron atom. Since the first synthesis in 2006,[1] they have been explored as a new class of functional pigments in light of their 14π aromatic networks, highly tunable optical and electrochemical properties, large effects of meso-aryl substituents, and relatively high fluorescence quantum yields.[2,3] Despite such great promise, numerous avenues of subporphyrin chemistry remain unexplored.

In the last two decades, fused porphyrin oligomers bearing multiple direct linkages have been demonstrated to display largely perturbed optical and electronic properties owing to conjugated π-networks.[4,5] Considering the rich chemistry of these porphyrins, it is natural to expect fused subporphyrin oligomers to be promising chromophores. As the first examples of fused dimers of ring-contracted porphyrinoids, the benzene-shared subphthalocyanine dimers $\mathbf{1}_{syn}$ and $\mathbf{1}_{anti}$ (Figure 1) were reported by the groups of Kobayashi and Torres independently, and both dimers showed considerably red-shifted and intensified Q-like bands.[6] Different from subphthalocyanines, subporphyrins bear meso-methine carbon atoms which may be used for direct fusion. However, the synthesis of a fused subporphyrin dimer has been thought to be challenging because of expected large strains.

Recently, we reported the synthesis of the meso–meso′ directly linked subporphyrin dimer **2a** by nickel(0)-mediated reductive homocoupling of meso-bromosubporphyrins.[7] We attempted oxidative fusion reactions of **2a** by methods used for the synthesis of fused porphyrins.[8] However, all these attempts failed, and ended in decomposition of **2a**, probably because of its fragile nature under oxidative conditions. These failures prompted us to consider an alternative non-oxidative route to the meso–meso′, *β*–*β*′ doubly linked subporphyrin dimer **3**. Therefore, we envisaged the synthetic route shown in Scheme 1. First, iridium-catalyzed regioselective *β*-borylation of the *B*-tolyl meso-free subporphyrin **4** with 0.8 equivalents of bis(pinacolato)diboron [$B_2(pin)_2$] in the presence of catalytic amounts of [{Ir(cod)OMe}$_2$] and 4,4′-di-*tert*-butyl-2,2′-bipyridyl (DTBPY) gave the 2-borylsubporphyrin **5** as an orange solid in 43% yield. In the next step, **5** was transformed into the 2-iodosubporphyrin **6** in 80% yield by iodination with *N*-iodosuccinimide and CuI.[9] Nickel(0)-mediated intermolecular reductive homocoupling of **6** furnished the *β*,*β*′-directly linked subporphyrin dimer **7** in 79% yield. The dimer **7** is expected to consist of two diastereomers, $\mathbf{7}_{DL}$ and $\mathbf{7}_{meso}$, and was actually obtained as an inseparable 1:1 mixture of $\mathbf{7}_{DL}$ and $\mathbf{7}_{meso}$. High-resolution atmospheric pressure chemical ionization time-of-flight mass spectrometry (HR-APCI-TOF-MS) has revealed the parent ion peak of **7** at *m*/*z* 1025.4656 (calculated for $[C_{72}H_{55}{}^{11}B_2N_6]^+$: 1025.4690) with an isotropic distribution consistent with the chemical composition. We then examined the meso-dibromination of **7** with *N*-bromosuccinimide (NBS), and it resulted in formation of a complicated mixture containing *B*-oxygenated products during aqueous work up, thus suggesting the occurrence of oxidative cleavage of the *B*-tolyl group. Thus, a diastereomeric mixture of **7** was converted into the *B*-methoxy-substituted subporphyrin dimer **8** in 90% yield as a 2:1 mixture of $\mathbf{8}_{DL}$ and $\mathbf{8}_{meso}$ upon treatment with trifluoroacetic acid (TFA) in CH_2Cl_2 and subsequent heating in methanol. The dimers

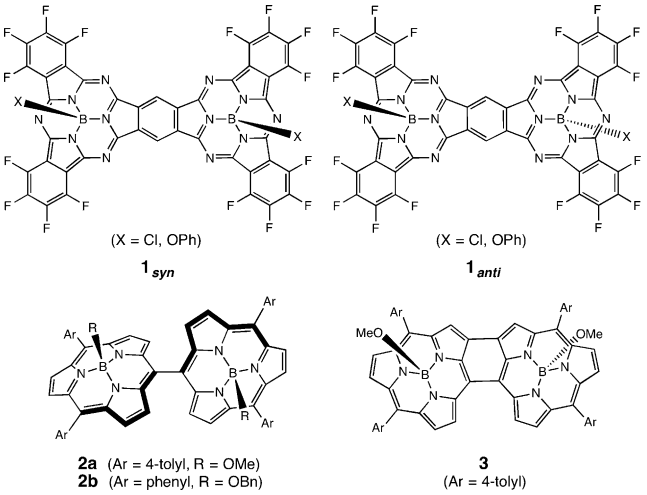

Figure 1. Compounds discussed in this paper.

[*] Y. Okuda, Dr. E. Tsurumaki, Prof. Dr. A. Osuka
Department of Chemistry, Graduate School of Science, Kyoto University, Sakyo-ku, Kyoto 606-8262 (Japan)
E-mail: osuka@kuchem.kyoto-u.ac.jp
J. Oh, Dr. J. Sung, Prof. Dr. D. Kim
Spectroscopy Laboratory for Functional π-Electronic Systems and Department of Chemistry, Yonsei University
Seoul 120-749 (Korea)
E-mail: dongho@yonsei.ac.kr

Supporting information for this article can be found under: http://dx.doi.org/10.1002/anie.201603759.

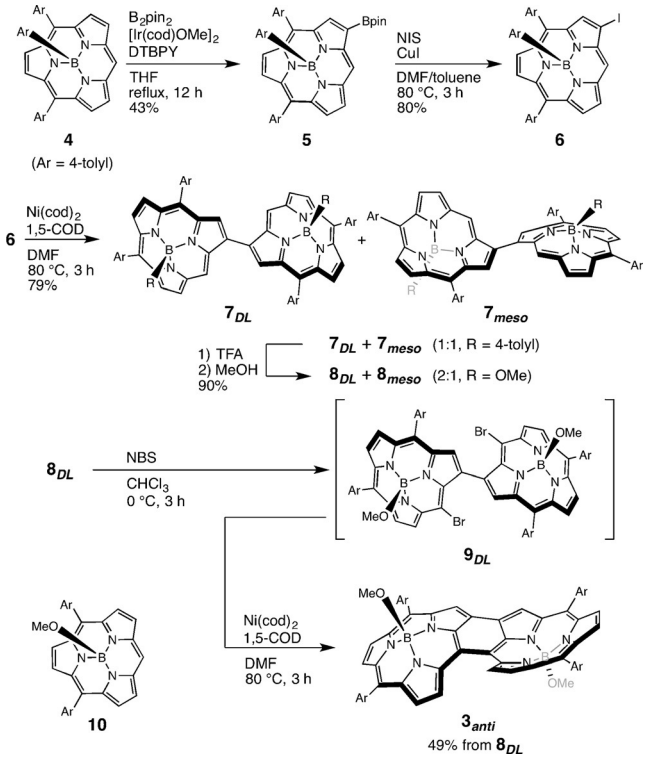

Scheme 1. Synthesis of fused subporphyrin dimer $\mathbf{3}_{anti}$. cod = 1,5-cyclooctadiene.

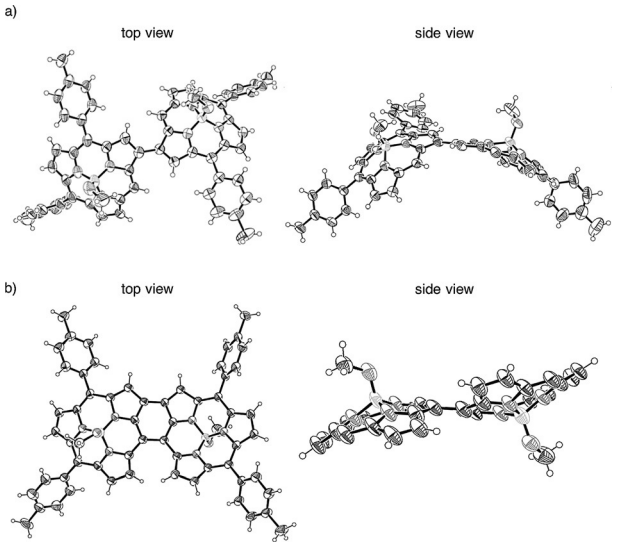

Figure 2. X-Ray crystal structures of a) $\mathbf{8}_{DL}$ and b) $\mathbf{3}_{anti}$.[13] The thermal ellipsoids are set at 50% probability, and one independent subporphyrin molecule in the asymmetric unit cell is represented.

$\mathbf{8}_{DL}$ and $\mathbf{8}_{meso}$ were inseparable by silica gel column chromatography, probably because of facile bowl inversion in the solution state. However, fortunately, slow recrystallization from CH_2Cl_2/methanol allowed preferential crystallization of $\mathbf{8}_{DL}$ as reddish orange crystals in an overall yield of 61% from **7**. Isomerization of pure $\mathbf{8}_{DL}$ in methanol at 50°C gave a diastereoisomeric 2:1 mixture of $\mathbf{8}_{DL}$ and $\mathbf{8}_{meso}$, thus suggesting the occurrence of the bowl inversion of subporphyrin,[10] and without methanol, isomerization was not observed.

The structure of $\mathbf{8}_{DL}$ was confirmed by X-ray diffraction analysis (Figure 2a). The asymmetric unit contains three independent subporphyrin dimers, with an average bowl depth of 1.44 Å. The average C_β–$C_{\beta'}$ bond length of $\mathbf{8}_{DL}$ is 1.44 Å, which is slightly shorter than the C_{meso}–$C_{meso'}$ bond length of **2b** (1.48 Å).[7] In addition, the average dihedral angle between the two subporphyrins is estimated to be 29.3° in $\mathbf{8}_{DL}$, and is distinctly smaller than that of **2b** (54.7°). The smaller dihedral angle of $\mathbf{8}_{DL}$ may be attributed to smaller steric congestion around the β-positions. On the basis of the crystal structure, the structures of $\mathbf{8}_{DL}$ and $\mathbf{8}_{meso}$ have been optimized by density functional theory (DFT) calculations at the level of B3LYP/6-311G(d) using the Gaussian 09 package.[10] These calculations have led to an estimation that $\mathbf{8}_{DL}$ is more stable than $\mathbf{8}_{meso}$ by 0.63 kcal mol^{-1}. This energy difference corresponds to a about a 2:1 equilibrium of $\mathbf{8}_{DL}$ and $\mathbf{8}_{meso}$ and is in line with the experimental observation. Characteristically, the ^{1}H NMR spectra of $\mathbf{8}_{DL}$ and $\mathbf{8}_{meso}$ revealed singlet signals resulting from the meso-protons and *B*-methoxy protons at $\delta = 9.33$ and 0.99 ppm and at $\delta = 9.24$ and 0.89 ppm, respectively, thus indicating almost free rotation along the C_β–$C_{\beta'}$ bond with respect to the NMR time scale at room temperature. These spectral features contrast with those of meso–meso linked dimer **2** and have been interpreted in terms of the restricted rotation along the C_{meso}–C_{meso} bond.[7]

In the next step, bromination of $\mathbf{8}_{DL}$ with 2 equivalents of NBS in $CHCl_3$ provided the meso,meso′-dibrominated subporphyrin dimer $\mathbf{9}_{DL}$ as a major product along with inseparable side products such as monobrominated and other dibrominated isomers. To our delight, a reaction of roughly separated $\mathbf{9}_{DL}$ with [Ni(cod)$_2$] in DMF at low concentration (ca. 6 mM) proceeded smoothly to give the meso–meso′, β–β', doubly linked subporphyrin dimer **3** in a two-step yield of 49% from $\mathbf{8}_{DL}$. The HR-APCI-TOF-MS spectrum of **3** revealed an intense borenium cation peak at *m*/*z* 871.3555 (calcd for $[C_{59}H_{41}{}^{11}B_2N_6O]^+$: 871.3540 [**3**-OMe]$^+$). The structure of **3** was revealed by X-ray crystallographic analysis to be roughly coplanar and wave-shaped (Figure 2b). Curiously, we obtained only a single *anti*-diastereomer, $\mathbf{3}_{anti}$. The selective formation of $\mathbf{3}_{anti}$ indicated that no bowl inversion occurred in the reaction sequence. Furthermore, $\mathbf{3}_{anti}$ did not undergo *anti–syn* isomerization, even under acidic conditions.[10] The asymmetric unit contains two independent dimers with an average bowl depth of 1.42 Å. The fused dimer $\mathbf{3}_{anti}$ shows a C_β–$C_{\beta'}$ bond length of 1.43 Å and a C_{meso}–$C_{meso'}$ bond length of 1.44 Å, which are, respectively shorter than the corresponding bonds in $\mathbf{8}_{DL}$ and **2b**. More distinct structural features of $\mathbf{3}_{anti}$ are dihedral angles between the two subporphyrin units: 22.9° at the meso-position and 17.3° at the β-position, which are smaller than those of **2b** and of $\mathbf{8}_{DL}$. These data indicate that $\mathbf{3}_{anti}$ has a more planar structure and is favorable for π-conjugation between two subporphyrin units. The optimized structures of $\mathbf{3}_{anti}$ and $\mathbf{3}_{syn}$ have been calculated by DFT method at the level of B3LYP/6–311G(d), thus showing that $\mathbf{3}_{syn}$ is seriously congested because of the closely located β-hydrogen atoms, and the total energy of $\mathbf{3}_{syn}$

is considerably higher than that of $\mathbf{3}_{anti}$ by as much as 6.1 kcal mol^{-1}, which may explain why only the *anti*-isomer was observed. The ^{1}H NMR spectrum of $\mathbf{3}_{anti}$ exhibits a singlet at $\delta = 1.39$ ppm resulting from the *B*-methoxy protons, and the ^{11}B NMR spectrum shows a signal at $\delta = -12.4$ ppm which represents the central boron atom. Both NMR signals are downfield shifted as compared with those of **2a** and $\mathbf{8}_{DL}$ ($\delta =$ 1.15 and −14.7 ppm, and $\delta = 0.99$ and −14.7 ppm, respectively), and has been interpreted in terms of its decreased diatropic ring current associated with effective electronic conjugation.

The UV/Vis absorption and fluorescence spectra of **10**, **2a**, $\mathbf{8}_{DL}$, and $\mathbf{3}_{anti}$ taken in CH_2Cl_2 are shown in Figure 3. The

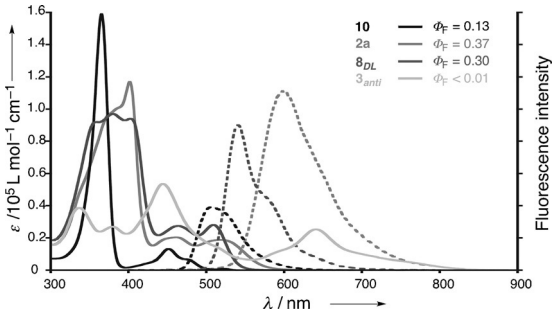

Figure 3. UV/Vis absorption (solid lines) and fluorescence (dashed lines) spectra of **10**, **2a**, $\mathbf{8}_{DL}$, and $\mathbf{3}_{anti}$ in CH_2Cl_2.

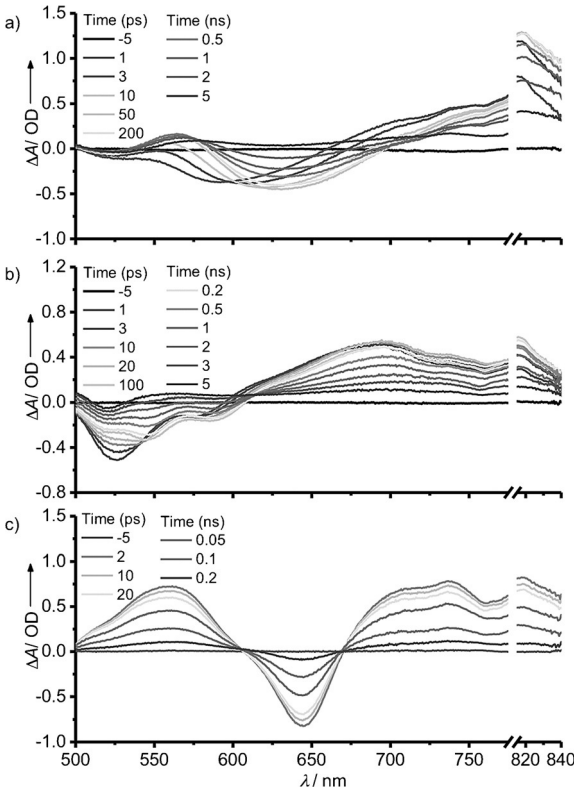

Figure 4. Transient absorption spectra of a) **2a**, b) $\mathbf{8}_{DL}$, and c) $\mathbf{3}_{anti}$ in toluene obtained by photoexcitation at $\lambda = 510$ and 650 nm, respectively.

dimer $\mathbf{8}_{DL}$ shows a split and red-shifted Soret-like band with maxima at $\lambda = 360$, 380, and 402 nm. The split Soret-like band of $\mathbf{8}_{DL}$ is accounted for in terms of exciton coupling between the two subporphyrins. The reduced dihedral angle between the two subporphyrin units induces the exciton interaction between quasi-orthogonal transition dipoles (i.e. B_y and B_z) of $\mathbf{8}_{DL}$, thus resulting in a strong higher-energy Soret-like band at $\lambda = 360$ nm. While **2a** exhibits broadened Q-like bands with a tail extending over 550 nm, $\mathbf{8}_{DL}$ shows rather sharp Q-like bands at $\lambda = 464$ and 509 nm. The fluorescence spectra of both **2a** and $\mathbf{8}_{DL}$ are red-shifted and substantially enhanced ($\Phi_F =$ 0.37 and 0.30, respectively) as compared to that of the monomer **10** ($\lambda_{max} = 504$ nm, and $\Phi_F = 0.13$). In contrast, the Stokes shift of $\mathbf{8}_{DL}$ (1160 cm^{-1}) is much smaller than that of **2a** (2360 cm^{-1}), thus indicating less structural relaxation of $\mathbf{8}_{DL}$ in the excited state. In contrast, the absorption spectrum of $\mathbf{3}_{anti}$ displays a broad and red-shifted Soret-like band at $\lambda = 444$ nm and considerably red-shifted Q-like band at $\lambda = 641$ nm with a tail reaching around $\lambda = 850$ nm. Like other doubly linked porphyrin dimers,[8c,11] these spectral features are mainly a result of the elongation of the π-conjugation. The fused dimer $\mathbf{3}_{anti}$ is practically nonfluorescent, probably because of its very fast relaxation of the S_1 state as discussed below.[12]

To investigate the excited-state dynamics, the transient absorption spectra of **2a**, $\mathbf{8}_{DL}$, and $\mathbf{3}_{anti}$ in toluene were obtained (Figure 4). The transient stimulated emission (SE) band of **2a** showed a gradual and distinct spectral shift resulting from the torsional relaxation after photoexcitation (Figure 4a). Since the direct meso–meso′ linkage of **2a** leads to efficient molecular orbital interaction between the two subporphyrins and hence the energetically stabilized Q_z state transition, the structural relaxation processes to give the coplanar geometry in the excited state are reflected in the SE bands as a clear dynamic Stokes shift. However, such a spectral shift was not so prominent in the SE bands of $\mathbf{8}_{DL}$, and is attributable to a small dihedral angle of the *β*–*β*′ linked subporphyrin dimer. Because of the small dihedral angle in the ground-state geometry, $\mathbf{8}_{DL}$ gets strong excitonic interaction in its Franck–Condon state, and leads to a relatively small dynamic shift in $\mathbf{8}_{DL}$. As shown in Figure 4c, the transient absorption spectra of $\mathbf{3}_{anti}$ did not show significant spectral changes but a very rapid decay with a time constant of 90 ps. The observed lack of the spectral shift can be ascribed to its rigid structure that restricts the structural relaxation in the excited state. The short S_1-state lifetime may be explained in terms of the reduced HOMO–LUMO energy gap which accelerates the nonradiative decay.

The electrochemical properties of $\mathbf{8}_{DL}$ and $\mathbf{3}_{anti}$ were examined by cyclic voltammetry and differential pulse voltammetry in CH_2Cl_2 containing 0.1 M nBu_4NPF_6 as a supporting electrolyte versus ferrocene/ferrocenium ion couple (Table 1). The quasireversible oxidation waves of **2a** were observed at 0.53 and 0.90 V and the reversible reduction wave was observed at −1.78 V. From these data, the electrochemical HOMO–LUMO gap of **2a** was estimated to be 2.31 eV. Compared to **2a**, $\mathbf{8}_{DL}$ shows irreversible oxidation waves at higher potential, 0.66 V, and two quasi-reversible reduction waves at −1.81 and −2.09 V, and thus its HOMO–LUMO gap

Table 1: Redox potentials and electrochemical HOMO–LUMO gaps for **10**, **2a**, $\mathbf{8}_{DL}$, and $\mathbf{3}_{anti}$.

compound	E_{ox2}/V	E_{ox1}/V	E_{red1}/V	E_{red2}/V	ΔE_{HL}/eV
10	–	0.61	−2.03	–	2.64
2a	0.90	0.53	−1.78	–	2.31
$\mathbf{8}_{DL}$	0.78	0.66	−1.81	−2.09	2.47
$\mathbf{3}_{anti}$	0.74	0.37	−1.35	−1.57	1.72

[a] Conditions: 0.1 M nBu$_4$NPF$_6$ as electrolyte. Working electrode: glassy carbon rod electrode. Counter electrode: Pt wire. Reference electrode: Ag/AgClO$_4$. Scan rate: 0.05 V s^{-1}. Potentials (V) vs. ferrocene/ferrocenium ion couple.

was estimated to be 2.47 eV. The larger HOMO–LUMO gap of $\mathbf{8}_{DL}$ than **2a** is in line with the blue-shifted absorption of $\mathbf{8}_{DL}$ as compared with that of **2a**. In contrast, $\mathbf{3}_{anti}$ shows two reversible oxidation waves at 0.37 and 0.74 V, and two reversible reduction waves at −1.35 and −1.57 V. The electrochemical HOMO–LUMO gap of $\mathbf{3}_{anti}$ is significantly smaller as compared with those of **2a** and $\mathbf{8}_{DL}$. The optimized molecular structures and molecular orbital diagrams of $\mathbf{8}_{DL}$ and $\mathbf{3}_{anti}$ were calculated at the B3LYP/6-311G(d) level. The orbital coefficients in LUMOs of $\mathbf{8}_{DL}$ and $\mathbf{3}_{anti}$ are spread over the two subporphyrins, thus indicating the effective electronic communication of the dimers (see the Supporting Information).

In summary, the meso–meso′, β–β′ doubly linked dimer $\mathbf{3}_{anti}$ was synthesized by intramolecular reductive fusion of a β–β′ linked meso,meso′-dibromosubporphyrin dimer. The dimer $\mathbf{3}_{anti}$ is the first example of fused subporphyrin oligomers, whereby only the *anti*-isomer was formed because of a large energetic stabilization as compared with the *syn*-isomer. The dimer $\mathbf{3}_{anti}$ displays a wavelike coplanar structure, a perturbed red-shifted absorption spectrum, highly reversible oxidation and reduction waves, a small HOMO–LUMO gap, and a short S_1-state lifetime. These properties can be attributed to the effective conjugation between the two subporphyrins. This work opens a door to fused arrays of subporphyrins of intriguing properties. More fabricated fused subporphyrin dimers and oligomers are actively being pursued in our laboratory.

Acknowledgments

The work at Kyoto University was supported by Grants-in-Aid from JSPS [Nos.: 25220802 (Scientific Research (S), 26620081 (Exploratory Research)]. The work at Yonsei University was supported by Global Research Laboratory (2013K1A1A2A02050183) through NRF of Korea.

Keywords: density functional calculations · dimerization · iridium · porphyrinoids · X-ray diffraction

How to cite: *Angew. Chem. Int. Ed.* **2016**, *55*, 9212–9215
Angew. Chem. **2016**, *128*, 9358–9361

[1] Y. Inokuma, J. H. Kwon, T. K. Ahn, M.-C. Yoo, D. Kim, A. Osuka, *Angew. Chem. Int. Ed.* **2006**, *45*, 961; *Angew. Chem.* **2006**, *118*, 975.

[2] a) Y. Inokuma, A. Osuka, *Dalton Trans.* **2008**, 2517; b) T. Torres, *Angew. Chem. Int. Ed.* **2006**, *45*, 2834; *Angew. Chem.* **2006**, *118*, 2900; c) A. Osuka, E. Tsurumaki, T. Tanaka, *Bull. Chem. Soc. Jpn.* **2011**, *84*, 679; d) C. G. Claessens, D. González-Rodríguez, M. S. Rodríguez-Morgade, A. Medina, T. Torres, *Chem. Rev.* **2014**, *114*, 2192.

[3] a) N. Kobayashi, Y. Takeuchi, A. Matsuda, *Angew. Chem. Int. Ed.* **2007**, *46*, 758; *Angew. Chem.* **2007**, *119*, 772; b) Y. Inokuma, Z. S. Yoon, D. Kim, A. Osuka, *J. Am. Chem. Soc.* **2007**, *129*, 4747; c) Y. Takeuchi, A. Matsuda, N. Kobayashi, *J. Am. Chem. Soc.* **2007**, *129*, 8271.

[4] a) D. Holten, D. F. Bocian, J. S. Lindsey, *Acc. Chem. Res.* **2002**, *35*, 57; b) M. O. Senge, M. Fazekas, E. G. A. Notaras, W. J. Blau, M. Zawadzka, O. B. Locos, E. M. N. Mhuircheartaigh, *Adv. Mater.* **2007**, *19*, 2737; c) M. Pawlicki, H. A. Collins, R. G. Denning, H. L. Anderson, *Angew. Chem. Int. Ed.* **2009**, *48*, 3244; *Angew. Chem.* **2009**, *121*, 3292; d) J. P. Lewtak, D. T. Gryko, *Chem. Commun.* **2012**, *48*, 10069.

[5] a) D. Kim, A. Osuka, *Acc. Chem. Res.* **2004**, *37*, 735; b) N. Aratani, D. Kim, A. Osuka, *Chem. Asian J.* **2009**, *4*, 1172; c) H. Mori, T. Tanaka, A. Osuka, *J. Mater. Chem. C* **2013**, *1*, 2500; d) T. Tanaka, A. Osuka, *Chem. Soc. Rev.* **2015**, *44*, 943.

[6] a) C. G. Claessens, T. Torres, *Angew. Chem. Int. Ed.* **2002**, *41*, 2561; *Angew. Chem.* **2002**, *114*, 2673; b) T. Fukuda, J. R. Stork, R. J. Potucek, M. M. Olmstead, B. C. Noll, N. Kobayashi, W. S. Durfee, *Angew. Chem. Int. Ed.* **2002**, *41*, 2565; *Angew. Chem.* **2002**, *114*, 2677; c) G. Zango, J. Zirzlmeier, C. G. Claessens, T. Clark, M. V. Martínez-Díaz, D. M. Guldi, T. Torres, *Chem. Sci.* **2015**, *6*, 5571.

[7] M. Kitano, J. Sung, K. H. Park, H. Yorimitsu, D. Kim, A. Osuka, *Chem. Eur. J.* **2013**, *19*, 16523.

[8] a) A. Tsuda, A. Osuka, *Science* **2001**, *293*, 79; b) A. Tsuda, H. Furuta, A. Osuka, *Angew. Chem. Int. Ed.* **2000**, *39*, 2549; *Angew. Chem.* **2000**, *112*, 2649; c) A. Tsuda, H. Furuta, A. Osuka, *J. Am. Chem. Soc.* **2001**, *123*, 10304; d) L. M. Jin, L. Chen, J.-J. Yin, C.-C. Guo, Q.-Y. Chen, *Eur. J. Org. Chem.* **2005**, 3994; e) A. K. Sahoo, Y. Nakamura, N. Aratani, K. S. Kim, S. B. Noh, H. Shinokubo, D. Kim, A. Osuka, *Org. Lett.* **2006**, *8*, 4141; f) B. J. Brennan, M. J. Kenny, P. A. Liddell, B. R. Cherry, J. Li, A. L. Moore, T. A. Moore, D. Gust, *Chem. Commun.* **2011**, *47*, 10034; g) C.-M. Feng, Y.-Z. Zhu, Y. Zang, Y.-Z. Tong, J.-Y. Zheng, *Org. Biomol. Chem.* **2014**, *12*, 6990.

[9] a) M. Kitano, Y. Okuda, E. Tsurumaki, T. Tanaka, H. Yorimitsu, A. Osuka, *Angew. Chem. Int. Ed.* **2015**, *54*, 9275; *Angew. Chem.* **2015**, *127*, 9407; b) A. L. S. Thompson, G. W. Kabalka, M. R. Akula, J. W. Huffman, *Synthesis* **2005**, 547; c) K. Fujimoto, H. Yorimitsu, A. Osuka, *Org. Lett.* **2014**, *16*, 972.

[10] The full list of the authors is given in the Supporting Information.

[11] a) A. Tsuda, A. Nakano, H. Furuta, H. Yamochi, A. Osuka, *Angew. Chem. Int. Ed.* **2000**, *39*, 558; *Angew. Chem.* **2000**, *112*, 572; b) J. H. Heo, T. Ikeda, J. M. Kim, N. Aratani, A. Osuka, D. Kim, *J. Phys. Chem. B* **2010**, *114*, 14528.

[12] One of the reviewers commented that the nonfluorescent nature of $\mathbf{3}_{anti}$ might derive from its aggregation. But aggregation of $\mathbf{3}_{anti}$ was not detected, even at 2.0×10^{-5} M (see Figure S4–2 in the Supporting Information).

[13] CCDC 1433125 ($\mathbf{8}_{DL}$) and 1433126 ($\mathbf{3}_{anti}$) contain the supplementary crystallographic data for this paper. These data can be obtained free of charge from The Cambridge Crystallographic Data Centre.

Received: April 19, 2016
Published online: June 21, 2016

